Research Square

Preprints are preliminary reports that have not undergone peer review.
They should not be considered conclusive, used to inform clinical practice,
or referenced by the media as validated information.

Engineered Biochars Enhances Carbon Dioxide Adsorption while Augmenting Soil Carbon Storage and Crop Yields in Semi-Arid Nigeria

Dahiru Wakili Habib
dwhabib.ssc@buk.edu.ng

Bayero University
Mansur Usman Dawaki
Bayero University
Bello Muhammad Shehu
Bayero University

Research Article

Keywords: Biochar modification, Carbon sequestration, CO_2 adsorption, Adsorption kinetics Aluminum toxicity, Semi-arid soils

Posted Date: July 13th, 2026

DOI: https://doi.org/10.21203/rs.3.rs-10082624/v1

License: This work is licensed under a Creative Commons Attribution 4.0 International License. Read Full License

Additional Declarations: No competing interests reported.

Abstract

Global warming, driven by anthropogenic greenhouse gas emissions, necessitates scalable carbon management strategies. Biochar has emerged as a promising tool for enhancing soil carbon sequestration. This study investigated the production, metal modification, and application of biochar in semi-arid Nigerian soils. Biochars from rice husk and sawdust were metalized with Mg and Al salts and tested for CO_2 adsorption and soil carbon sequestration capacity. Thermogravimetric analysis revealed significantly higher CO_2 adsorption in Mg-loaded biochar (83 mg g^{-1} at 30°C) compared with unmodified biochar (63 mg g^{-1}). Adsorption kinetics were best described by the Avrami model, indicating mixed physisorption–chemisorption mechanisms under laboratory conditions. Field trials over two growing seasons showed substantial increases in total soil carbon sequestration, with Mg-biochar consistently outperforming Al-biochar and controls. The application of 10 t ha^{-1} of engineered biochar resulted in immediate carbon gains, driven by both the direct addition of recalcitrant pyrogenic carbon and secondary inorganic carbonate formation, while Mg-modification further reduced net soil CO_2 efflux. However, an environmental safety assessment indicates that Al-modified biochars pose potential biotoxicity risks in acidic or semi-arid soils, making Mg-modification the preferred agronomic strategy. Biochar application enhanced groundnut yields by 33–47%, demonstrating co-benefits for soil fertility and productivity. These findings highlight Mg-engineered biochar as a scalable strategy for climate change mitigation and sustainable agriculture.

Introduction

Human activities have significantly increased the emission of greenhouse gases like CO_2, CH_4, and N_2O, intensifying global warming [11]. The primary driver is the excessive accumulation of atmospheric carbon due to accelerated climate change. To mitigate these effects, it is essential to restore the natural carbon balance by enhancing carbon sequestration efforts [9]. Since CO_2 is the most significant contributor to global warming, there is a growing need to invest in technologies that reduce its emissions and boost carbon sinks to achieve climate goals [3].

Climate change severely affects agriculture, especially in low- and middle-income countries, through increased droughts, floods, pests, and diseases [5]. Additionally, unsustainable farming methods like monoculture and soil tillage have depleted soil carbon, creating a global "carbon debt" with serious implications for soil health, crop productivity, and climate stability [6, 13]. Similarly, the average concentration of organic carbon is low throughout the Sudan Savannah in Nigeria. This low level of organic matter is attributed to the continuous intensive cropping practiced in the area without the provision of proper means to replenish the organic matter [10].

In agroforestry research, one of the more recent strategies explored for enhancing carbon sequestration in both plants and soil is the use of biochar [16, 17]. When applied as a soil amendment, biochar can also help reduce greenhouse gas emissions from the soil. While unprocessed biochar has limited capacity to adsorb carbon, various modification techniques have been developed to improve its performance, with varying levels of effectiveness.

Most of the researches conducted using modified biochar were restricted to CO_2 adsorption from the atmosphere not the soil. This study aims to cover this gap and use this engineered biochar in the soil, i.e. to see how much of the carbon will be sequestered in cultivated a soil and CO_2 adsorbed from the soil environment, especially in our environment (semi-arid) that is vulnerable to massive weather changes.

Most research conducted using modified biochar has been restricted to CO_2 adsorption under controlled laboratory conditions, lacking field-scale validation. This study aims to bridge this gap by applying engineered biochars in semi-arid soils to quantify the enhancement of the total soil carbon pool and the reduction of soil CO_2 efflux. Specifically, it was hypothesized that metal impregnation (Mg and Al) would significantly enhance the CO_2 adsorption capacity of rice husk and sawdust biochars. Furthermore, the application of these engineered biochars would lead to a quantifiable increase in stable soil carbon sequestration, while evaluating the critical environmental safety trade-offs associated with metal leaching, particularly aluminum toxicity.

Materials and methods

Description of the study area

This research was conducted at Center for Dryland, Agriculture, research, and teaching farms Located between latitude 11.97932° to 11.98194°N, and longitude 8.41245° to 8.42205°E, with varying altitudes ranging from 427 to 434 m above sea level. The climate of the study area is the tropical wet and dry type [1], with a mean annual rainfall of approximately 500–760 mm, all of which falls between June and October, and a mean daily temperature range of 25 ± 7°C.

Biochar production, processing and analyses.

The biochar used in this study was produced using locally available materials (rice husk and saw dust) as feedstock. Biochar was produced by slow pyrolysis in a custom-built fixed-bed reactor. The feedstock was heated at a rate of 10°C min^{-1} to a final temperature of 750–800°C and held for a residence time of 2 hours under a continuous N_2 flow (2 L min^{-1}) to ensure anaerobic conditions. The average biochar yield was 35%. The resulting biochar was ground with a pestle and mortar and passed through a 1mm sieve. The biochar properties were evaluated according to the IBI International Standard. The biochar properties were evaluated according to the [14].

Soil analysis

Soil pH was measured using a JENWAY 3520 glass electrode pH meter at a 1:2.5 soil-to-solution ratio, both in distilled water and 1.0M KCl. Electrical conductivity (EC) was assessed with a DDS-307 conductivity meter. Organic carbon content was analyzed through the Walkley and Black [15] wet oxidation

method. Total nitrogen was measured using 0.5M K_2SO_4 extraction and subsequent rapid colorimetric analysis. Exchangeable cations (Ca, Mg, K, and Na) were extracted with 1N ammonium acetate (pH 7.0) as outlined by [2], and their concentrations were determined using a BUCK SCIENTIFIC 210 VGP atomic absorption spectrophotometer.

Metal Impregnation

To produce metal-enriched biochar, the method outlined by [18] was followed. Magnesium nitrate hexahydrate ($Mg(NO_3)_2·6H_2O$) and aluminum nitrate nonahydrate ($Al(NO_3)_3·9H_2O$) were used as metal sources. These salts were dissolved in deionized water to prepare 5% metal solutions. Biochar was added to the solution at a 1:10 (w/v) ratio and stirred for 2 hours. The pH of the slurry was adjusted to 10 using 0.1M NaOH to facilitate metal precipitation onto the biochar surface. The mixture was then oven-dried at 105°C for 24 hours. The resulting metalized biochar was washed with deionized water until the wash water was nitrate-free (tested with diphenylamine) and then dried again. The target metal loading was 5% by weight.

Land preparations and biochar application

The experimental site was manually cleared of vegetation, and the soil was plowed and harrowed to a depth of 20 cm. The experiment was laid out in a split-plot design with three replications. The plot size was 4m x 5m. Ground biochar was evenly applied to the plots by hand at a rate of 10 t ha^{-1} and then mechanically incorporated into the topsoil. The trial was carried out over two growing seasons, using groundnut (Arachis hypogaea L., var. SAMNUT-24) as the test crop, planted at a density of 75 cm x 25 cm. A basal fertilizer dose of 20 kg N, 40 kg P_2O_5, and 40 kg K_2O per hectare was applied to all plots. Supplementary irrigation was provided as needed to prevent water stress. Soil samples were collected from each plot at a depth of 0–20 cm at three time points: pre-planting, post-harvest year 1, and post-harvest year 2

Experimental design

A 2 × 3 treatment combination was implemented using a split plot design. The main treatment was biochar material, and the sub-treatment was biochar engineering. The experiment was replicated three times.

Carbon dioxide adsorption

Carbon dioxide (CO_2) adsorption tests were performed following the method of [18] using a thermogravimetric analyzer (TGA, SDTQ-600). Biochar samples were placed in the TGA pan and heated under a nitrogen flow (75 ml/min) at a rate of 20°C/min until reaching 110°C, where they were held for 15 minutes to eliminate moisture and storage-related impurities. The temperature was then adjusted to the target adsorption temperature (30, 40, or 50°C). After stabilization, the nitrogen flow was replaced with CO_2 (75 ml/min), and the temperature was maintained isothermally for 60 minutes to allow for adsorption.

Regeneration study

A regeneration study was carried out using cyclic adsorption–desorption tests on the biochar sorbent, repeated across five cycles. Weight changes were monitored throughout to evaluate any decline in CO_2 adsorption capacity. To improve accuracy, each test was conducted in duplicate.

Carbon dioxide capture kinetics

To quantitatively analyze the kinetics of CO_2 adsorption on various adsorbents and determine the potential adsorption mechanism, three kinetic models were applied: the pseudo-first-order, pseudo-second-order, and Avrami models. These models are represented by the following equations:

Pseudo-first-order model:

$$qt = qe * (1 - exp(-k1 * t))$$

where qe and qt (mg/g) represent the amount of CO_2 adsorbed at equilibrium and at a specific time t (min), respectively. The parameter k1 (min^{-1}) denotes the rate constant for the pseudo-first-order kinetic model.

Pseudo-second-order model:

$$qt = (k2 * qe^2 * t) / (1 + k2 * qe * t)$$

where qe and qt (mg/g) refer to the quantities of CO_2 adsorbed at equilibrium and at a specific time t (min), respectively, while k2 ($g·mg^{-1}·min^{-1}$) is the rate constant for the pseudo-second-order kinetic model.

Avrami model:

$$qt = qe * (1 - exp(-(k_A * t)^n_A))$$

where qe and qt (mg/g) represent the equilibrium and instantaneous CO_2 adsorption capacities, respectively. k_A (min^{-1}) is the Avrami rate constant, and n_A is the Avrami exponent, which provides insight into the adsorption mechanism.

Carbon sequestration determination

Estimation of carbon sequestration was done using a relationship described by [19]. The relation estimate the sequestration of carbon from the baseline and endline soil data collected.

$$\mathrm{RCSR} = \frac{\mathrm{cmtn} - \mathrm{cmto}}{\mathrm{tn} - \mathrm{to}} \quad 5$$

Where RCSR is real carbon sequestration rate in t ha^{-1} yr^{-1}

Cmtn is carbon stock in t ha^{-1} in treatment at endline

Cmto is carbon stock in t ha^{-1} in treatment at baseline

tn-to is time interval

Carbon stock (kg ha^{-1}) = *D*CC*BD*10000* 6

Where

BD denotes the bulk density (g cm^{-3}) of layer i.

*C*i represents the fraction of carbon (g C g^{-1})

D thickness of the layer (depth in cm).

Soil carbon flux measurement

The soil carbon flux was measured using a CIRAS-2 infrared gas analysis system equipped with an SRC-1 soil respiration chamber. This system, capable of operating in both open and closed configurations, employs a measurement probe inserted 3 cm into the soil. The SRC-1 has a chamber with dimensions of 78 cm^2 area and 1170 cm^2 volume. Each measurement point requires 120 seconds to capture soil CO_2 respiration data. Measurements were conducted between 9:00 am and 2:00 pm to observe changes in soil carbon dioxide fluxes, as this time frame aligns with midday CO_2 efflux values, which are indicative of daily averages in vegetation areas [20].

Data Analysis

Data were analyzed using a split-plot mixed model Analysis of Variance (ANOVA). Biochar material (sawdust, rice husk) was treated as the main-plot factor, biochar engineering (Mg-modified, Al-modified, control) as the sub-plot factor, and year (two growing seasons) as a repeated measure. Replications (n = 3 blocks) were treated as a random effect. The model structure was as follows:

$$Y = \mu + Block + Material + Block * Material\ (Error\ A) + Engineering + Material * Engineering + Year + Material * Ye$$

An autoregressive covariance structure (AR1) was used to model the correlation between repeated measurements over the two years. Analyses were conducted in JMP® 17 (SAS Institute, Cary, NC, USA) and verified in R (lme4 package). Model assumptions were checked using the Shapiro–Wilk test for normality and Levene's test for homogeneity of variances. Post-hoc pairwise comparisons were conducted using Tukey's HSD (α = 0.05). A summary of the ANOVA table is provided in the supplementary materials.

Result and discussion

Result

Tables 1 and 2 show the summary statistics of the physical and chemical composition of the biochar used in the research. The pH both in H_2O and $CaCl_2$ of the biochar fall within the alkaline class having a mean concentration of 7.69 (H_2O) and 7.33 9 ($CaCl_2$). The standard deviation and coefficient of variation is as shown in the table. Electrical conductivity of the material is low. The percentage carbon content of the biochar is 83.72 (Table 1). Sulphur, oxygen and hydrogen were as shown in Table 1. The H/C and O/C ratios are very low (Table 1). Exchangeable bases Mg, Ca, K and Na where low to medium. The mean concentration of total nitrogen and available P of the biochar material was as shown in Table 1. Micronutrient (Cu, Mn, Fe and Zn) were found to also be low to medium. Cr was found to have a mean concentration of 0.08 mg kg^{-1} in the biochar material. Pb and Cd were not detected in the biochar material by the machine. The variation and deviation amongst the all the parameters is portrayed in the table. The highest variation was found in Zn with % CV of more than 10.

The ash and volatile matter content or yield were higher in rice husk relative to saw dust Table 3.

Table 1
Elemental Composition of Biochar

Parameters	Minimum	Maximum	Mean	SD	CV (%)
pH (H_2O)	7.61	7.76	7.69	0.11	1.38
pH $CaCl_2$	7.23	7.43	7.33	0.23	1.43
EC (dSm^{-1})	0.03	0.05	0.04	0.01	28.28
C (%)	83.23	84.21	83.72	0.69	0.83
O (%)	12.11	12.21	12.16	0.07	0.58
H (%)	3.91	4.49	4.20	0.41	9.76
H/C	0.05	0.06	0.06	0.00	7.44
O/C	0.15	0.15	0.15	0.00	1.43
AP (mg kg^{-1})	18.65	18.76	18.71	0.08	0.42
K (cmol kg^{-1})	0.81	0.82	0.82	0.01	0.69
Mg (cmol kg^{-1})	0.29	0.30	0.29	0.00	0.97
Ca (cmol kg^{-1})	2.68	2.68	2.68	0.00	0.11
Na (cmol kg^{-1})	0.50	0.51	0.50	0.01	2.25
Mn (mg kg^{-1})	11.61	12.11	11.86	0.35	2.96
TN (g kg^{-1})	0.94	1.00	0.97	0.04	4.37
S (%)	0.07	0.07	0.07	0.00	3.05
Zn (mg kg^{-1})	2.28	2.29	2.29	0.00	0.22
Cr (cmol(+) kg^{-1})	0.08	0.09	0.08	0.00	3.37
Cu (mg kg^{-1})	0.67	0.68	0.68	0.00	0.63
Fe (mg kg^{-1})	31.90	31.91	31.90	0.01	0.02
Cd (cmol(+) kg^{-1})	ND				
Pb (mg kg^{-1})	ND				

ND = Not detected, SD = Standard deviation, CV = Coefficient of variation

Table 2
Proximate Analysis

Parameters	Min	Max	Mean	SD	CV (%)
Volatile Matter (%)	25.6	26.1	25.8	0.35	1.37
Ash (%)	5.7	5.87	5.79	0.12	2.08
SD = Standard deviation, CV = Coefficient of variation					

Physical and chemical properties of the study soil

Table 3 presents the baseline physical and chemical properties of the experimental soil. The soil is a sandy loam with a slightly acidic pH. The bulk density was relatively high, and the organic carbon and total nitrogen levels were low, which is typical for intensively cultivated soils in the Sudan Savannah region of Nigeria. Exchangeable bases such as Ca, Mg, and K are rated low to moderate, whereas sodium content averages 0.50 $cmol^{(+)}$ kg. Sulphur content is classified as high. Among the parameters, potassium exhibits the highest variation. Zinc, copper, and lead concentrations are notably low in the study soil, as depicted in Table 3.

Surface area and porosity of the biochars

Table 4 displays the surface area and porosity of the biochar pre- and post-engineering. Following the successful integration of metal ions into the biochar structure and pH adjustment, the surface area of the biochars was re-examined. The table illustrates that, all materials exhibited greater surface area than the control. This augmentation trend is consistent across both the metals. A notable effect ($p < 0.05$) was observed in surface area, total pores, micro, and

macro porosity. However, no significant difference was noted in pore size. Additionally, a highly significant difference was observed in the interaction between metal ions and biochar materials.

Table 3
Physical and Chemical Properties of the study soil

Parameters	Minimum	Maximum	Mean	SD	CV (%)
Sand (%)	65	69	67	1.41	4.23
Silt (%)	22	26	24	2.83	11.79
Clay (%)	6	10	8	0.04	11.11
Textural class	Sandy loam				
BD (g cm^{-3})	1.49	1.54	1.51	0.04	2.33
pH (H_2O)	6.45	6.71	6.58	0.18	2.79
pH ($CaCl_2$)	6.23	6.54	6.39	0.22	3.43
EC (dSm^{-1})	0.02	0.07	0.05	0.04	7.8
Mg (cmol kg^{-1})	1.92	2.87	2.40	0.67	8.9
K (cmol kg^{-1})	0.76	1.02	0.89	0.14	15.37
Na (cmol kg^{-1})	0.67	0.76	0.72	0.06	8.9
Ca (cmol kg^{-1})	6.4	7.88	7.14	1.04	14.65
O.C (g kg^{-1})	3.69	4.11	3.90	0.30	7.61
TN (g kg^{-1})	0.73	1.43	1.08	0.49	4.58
Available P (mg kg^{-1})	15.95	23.56	19.76	0.21	2.7
Fe (mg kg^{-1})	23.86	31.56	27.71	5.44	5.5
Zn (mg kg^{-1})	1.06	1.98	1.52	0.65	4.27
Cu (mg kg^{-1})	0.76	0.92	0.84	0.11	13.46
Pb (mg kg^{-1})	0.017	0.04	0.029	0.02	5.71
S (mg kg^{-1})	6	7.55	6.78	1.09	13.45
ND = Not detected, SD = Standard deviation, CV = Coefficient of variation					

X-ray Diffraction

XRD patterns (Fig. 1) confirmed the successful incorporation of Mg and Al. Mg-biochar exhibited distinct peaks at 36–38° 2θ corresponding to MgO, providing basic sites for CO_2 chemisorption. Al-biochar showed reflections at 20° and 38° 2θ from Al_2O_3, which improved stability but contributed fewer basic sites.

Fourier-transform infrared spectroscopy (FTIR)

FTIR spectra (Fig. 2) revealed carbonate stretching vibrations (1400–1500 cm^{-1}) in Mg-biochar, confirming strong chemisorption, while Al-biochar displayed Al–O bands (600–800 cm^{-1}).

Fourier-transform infrared spectroscopy (FTIR)

FTIR spectra (Fig. 2) revealed carbonate stretching vibrations (1400–1500 cm^{-1}) in Mg-biochar, confirming strong chemisorption, while Al-biochar displayed Al–O bands (600–800 cm^{-1}).

Scanning electron microscopy (SEM)

SEM images (Fig. 3) showed unmodified biochar with open porous channels. Mg-modified biochar exhibited crystalline MgO deposits partially blocking pores but enhancing surface reactivity. Al-modified biochar displayed heterogeneous surfaces with dispersed Al_2O_3. These morphological changes align with the adsorption performance trends.

Table 4
Surface Area and Porosity Analysis of the Biochar

Parameters	Surface area ($m^2 g^{-1}$)	Total pore volume ($cm^3 g^{-1}$)	Micropore volume ($cm^3 g^{-1}$)	Microporosity fraction (%)	Pore size (Å)
Biochar material					
Rice husk	265.77^{d}	0.141^{bcd}	0.104^{bc}	74.12^{a}	21.229
Saw dust	402^{bc}	0.123^{bcd}	0.121^{ab}	64.22^{b}	24.001
SE±	75.661	0.005	0.005	8.012	1.641
Level of significance	*	*	**	*	NS
P-value	0.032	0.05	0.001	0.045	0.34
Engineering					
Mg	564^{a}	0.172^{bc}	0.143^{ab}	80.73^{a}	21.523
Al	521^{a}	0.198^{ab}	0.159^{b}	80.74^{a}	19.937
Control	401^{bc}	0.134^{bcd}	0.111^{a}	62.79^{b}	23.55
SE±	95.626	0.005	0.005	8.012	1.641
Level of significance	*	*	**	*	NS
P-value	0.043	0.05	0.001	0.045	0.34
Interaction					
Material x Metals	**	**	**	**	**

SE ± = Standard error of Means. Values followed by the same letter are not statistically different.

Interaction between biochar materials and engineering on surface area and porosity of biochar

Table 5 displays the interaction between biochar materials and engineering on surface area and porosity. The findings shows a significant difference ($p < 0.05$) in the surface area, total pore volume and micro porosity fraction of the biochar. A significant difference was observe in micropore volume of the biochar. Magnesium (Mg) loaded biochar showed the most significant change in these physical characteristic of the material, succeeded by Al.

Table 5: Interaction between biochar materials and engineering on surface area and porosity of biochar

Materials	Engineering	Surface area ($m^2 g^{-1}$)	Total pore volume ($cm^3 g^{-1}$)	Micropore volume ($cm^3 g^{-1}$)	Microporosity fraction (%)
Saw dust	Mg	564^{a}	0.172^{b}	0.143^{a}	80.73^{a}
Saw dust	Al	521^{b}	0.198^{a}	0.159^{b}	80.74^{a}
Saw dust	Control	401^{bc}	0.134^{bc}	0.111^{bc}	62.79^{b}
Rice husk	Mg	544^{a}	0.181^{bc}	0.150^{a}	82.12^{a}
Rice husk	Al	501^{ab}	0.191^{ab}	0.163^{b}	79.44^{a}
Rice husk	Control	409^{b}	0.144^{bcd}	0.115^{bc}	61.19^{b}

Values followed by the same letter are not statistically different.

Carbon Dioxide (CO_2) Adsorption Capacity of Metal Loaded Biochars at different Temperature

The CO_2 adsorption capacity of the biochars at different temperatures is presented in Table 6. Metal impregnation significantly ($p < 0.05$) enhanced the CO_2 adsorption capacity of both rice husk and sawdust biochars. Mg-modified biochars consistently showed the highest adsorption capacity, with the Mg-rice husk biochar reaching 83 mg g^{-1} at 30°C. This is likely due to the introduction of basic metal oxides (e.g., MgO) on the biochar surface, which act as active sites for CO_2 chemisorption.

Table 6: Carbon dioxide (CO_2) adsorption capacity (mg g^{-1}) of metal loaded biochars at different temperatures

Parameters	Temperature (°C)		
	30	40	50
Biochar material			
Saw dust	71.74[b]	62.12[a]	43.78a
Rice husk	63.61[a]	51.76[b]	37.19[b]
SE±	12.21	10.76	15.79
Level of Significance	**	**	**
P-value	<0.001	<0.001	<0.001
Engineering			
Mg	76.5 [ab]	69.41[b]	57.11[b]
Al	74.1[b]	60.88[b]	51.76[bc]
Control	61.2[bc]	54.33[abc]	31.81[cde]
SE±	16.36	21.56	10.19
Level of Significance	**	**	**
P-value	<0.001	<0.001	<0.001
Interaction			
Biochar material x Engineering	*	*	*

Values followed by the same letter are not statistically different.

Interaction between Biochar Material and Metals on Carbon Adsorption at different Temperature

Table 7 displays the interaction between biochar materials and engineering on adsorption at different temperatures. The findings showed a highly significant difference ($p < 0.001$) on the adsorption capacity of the biochar at different temperatures with biochar engineering. The highest adsorption was observed at 30°C, which decreases as the temperature increases.

Table 7: Interaction between biochar material and engineering on carbon adsorption at different temperatures

Parameters		Temprature (°C)		
	Engineering			
		30	40	50
		mg g^{-1}		
Saw dust	Mg	83[a]	71.64[a]	57.76[a]
Saw dust	Al	78.01[b]	60.1[b]	51.28[bc]
Saw dust	Control	63.31[c]	54.21[bcd]	41.23[c]
Rice husk	Mg	80[a]	68.47[ab]	52.64[bc]
Rice husk	Al	76.01[bc]	60.1[b]	49.81[bc]
Rice husk	Control	63.55[c]	49.97[d]	33.65[e]

Values followed by the same letter are not statistically different.

Regenerability of the engineered biochar

The regeneration study (Fig. 4) showed that the engineered biochars maintained high adsorption capacity over five adsorption-desorption cycles, with less than a 5% decrease in performance. This indicates good stability and reusability of the adsorbents.

Parameters of pseudo-first order, pseudo-second order and Avrami kinetic models.

As shown in Table 8 for SD and RH, the kinetics of CO_2 adsorption were best explained by pseudo-first and Avrami kinetic models for both the engineered and the pristine biochar forms. Both models showed high correlation between calculated and experimental values over all the investigated temperature, than the pseudo-second order which over estimated and under estimated some of the values in both the SD and RH biochars. The (constant) k values across the experimental data sets decreased with increase in temperature in both the biochar materials.

Table 8: Parameters of pseudo-first order, pseudo-second order and Avrami kinetic models.

Parameters	Temperature (°C)	Experimental	Pseudo first order			Pseudo Second order			Avrami			
		qe,exp ($mg\ g^{-1}$)	qe,cal ($mg\ g^{-1}$)	k_1 (s^{-1})	R^2	qe,cal ($mg\ g^{-1}$)	k_2 (s^{-1})	R^2	qe,cal ($mg\ g^{-1}$)	k_A (s^{-1})	n_A	R^2
SD Mg-loaded	30	83.65	83.13	0.1486	0.9956	94.65	0.0086	0.8956	83.55	0.5486	0.4956	0.9
	40	71.64	71.43	0.1110	0.9976	64.74	0.0030	0.8576	71.60	0.1870	0.9576	0.9
	50	57.76	56.99	0.0946	0.9953	52.96	0.046	0.8953	57.36	0.0946	0.8987	0.9
SD Al-loaded	30	78.01	77.89	0.0958	0.9976	79.81	0.0058	0.8976	77.71	0.1758	0.7001	0.9
	40	60.10	59.91	0.0822	0.9966	57.41	0.0022	0.9136	59.31	0.0422	0.5613	0.9
	50	51.28	51.21	0.0749	0.9982	52.98	0.0041	0.8962	50.62	0.0249	0.0962	0.9
SD Control	30	62.71	62.21	0.0995	0.9976	60.78	0.0054	0.9076	62.01	0.0995	1.0176	0.9
	40	52.12	51.92	0.0858	0.9963	50.27	0.0058	0.8983	52.07	0.0758	0.8983	0.9
	50	43.78	42.80	0.0722	0.9981	42.82	0.0022	0.9487	43.58	0.0322	0.9798	0.9
RH Mg-loaded	30	76.50	75.99	0.1476	0.9956	77.54	0.0086	0.8956	76.65	0.5486	0.8956	0.9
	40	69.41	68.93	0.1210	0.9976	61.43	0.0030	0.8576	69.45	0.1870	0.8576	0.9
	50	57.11	56.79	0.0946	0.9953	59.12	0.0046	0.8953	57.18	0.0946	0.8953	0.9
RH Al-loaded	30	74.1	73.91	0.0798	0.9976	71.78	0.0058	0.9476	74.12	0.1758	0.8976	0.9
	40	60.88	60.81	0.0682	0.9966	60.56	0.0022	0.9736	60.78	0.0722	0.9136	0.9
	50	51.76	51.70	0.0349	0.9982	51.93	0.0041	0.8967	51.78	0.0449	0.8962	0.9
RH Control	30	63.61	63.59	0.0925	0.9967	60.81	0.0054	0.9476	60.59	0.0695	0.9076	0.9
	40	51.76	51.74	0.0798	0.9939	52.25	0.0058	0.8783	51.74	0.0458	0.8983	0.9
	50	37.19	37.16	0.0424	0.9989	37.87	0.0022	0.9587	37.12	0.0122	0.9487	0.9

Values followed by the same letter are not statistically different.

Carbon Sequestration of the Pristine and Engineered Biochar

Table 9 presents data on the potential for carbon sequestration by both pristine and modified forms of biochar over different growing seasons and application rates, as evidenced by changes in carbon stock. The results indicate a highly significant difference ($p < 0.001$) in the effectiveness of biochar modification, with Mg-loaded biochar exhibiting the highest carbon sequestration. Additionally, there was a highly significant difference ($p < 0.017$) in carbon sequestration among different biochar materials across seasons with saw dust slightly sequestering more carbon. Consequently, treatments resulted in greater carbon sequestration during the initial growing period over the second growing season. Furthermore, there was a significant interaction (**), as indicated in Table 9, between biochar materials and other components.

Soil CO_2 flux

Soil CO_2 flux was significantly affected by the biochar treatments (Fig. 5). While all biochar-amended soils initially showed a slight increase in CO_2 efflux (a priming effect), the engineered biochars, particularly the Mg-modified types, led to a net reduction in CO_2 emissions over the course of the growing seasons compared to the control.

Table 9
Carbon sequestration potential of pristine and engineered biochars across two growing seasons (t C ha^{-1} yr^{-1}).

Parameters	Carbon sequestration (t C ha^{-1} yr^{-1})
Biochar material	
Rice husk	22.21[b]
Saw dust	26.77[a]
SE±	0.46
Level of significance	**
P-value	0.017
Engineering	
Mg	30.49[a]
Al	19.92[b]
Control	
SE±	0.25
Level of significance	**
P-value	0.001
Year	
1	27.42[a]
2	25.73[b]
SE±	0.17
Level of significance	*
P-value	0.022
Interaction	
Biochar material x engineering	**
Biochar material x year	**
Biochar material x engineering x year	**

Values followed by the same letter are not statistically different.

Interaction of Biochar Material by Engineering on Carbon Sequestration

Table 10 displays the interaction between biochar materials and metals impregnation. The findings shows a highly significant difference ($p < 0.001$) in the efficacy of biochar modification, with Mg-loaded biochar showing the most significant carbon sequestration, succeeded by Al whereas pristine biochar displayed the least sequestration potential. This pattern remains consistent across different biochar materials (RH and SD).

Table 10
Interaction between biochar materials and engineering

Parameters	Engineering	Carbon Sequestration (t C ha^{-1} yr^{-1})
Saw dust	Mg	42.40[a]
Saw dust	Al	36.55[b]
Saw dust	Control	23.50[d]
Rice husk	Mg	39.70[a]
Rice husk	Al	32.35[b]
Rice husk	Control	22.97[c]

Values followed by the same letter are not statistically different.

Interaction of Biochar Material and Growing Seasons on Carbon Sequestration

Table 11 shows the interaction between biochar materials across two growing seasons. The result shows a highly significant distinction ($P < 0.001$) in carbon sequestration throughout the two growing seasons. The findings indicate that the most substantial carbon sequestration occurred during the initial growing season.

Table 11
Interaction between biochar materials and growing seasons on Carbon Sequestration

Parameter	Year	Carbon Sequestration(t C ha^{-1} yr^{-1})
Saw dust	1	49.40^{a}
Rice husk	1	37.59^{b}
Saw dust	2	28.49^{c}
Rice husk	2	26.96^{d}

Values followed by the same letter are not statistically different.

Interaction of Biochar Material and Growing Seasons

Table 12 depict the nested effect of biochar material alongside various modification methods across two growing seasons. The result shows a highly significant distinction ($P < 0.001$) in carbon sequestration between unaltered and modified biochar materials throughout the two growing seasons. The findings indicate that the most substantial carbon sequestration occurred during the initial growing season. Following this, biochar modified with Mg demonstrated the highest carbon sequestration, followed by Al, whereas control exhibited the least sequestration potential. This pattern remained consistent across all biochar materials.

Table 12: Interaction of Biochar Material, Engineering and Growing Seasons

Material	Engineering	Year	Carbon Sequestration (t C ha^{-1} yr^{-1})
Saw dust	Mg	1	56.20^{a}
Saw dust	Al	1	45.25^{cd}
Saw dust	Control	1	29.74^{ghi}
Rice husk	Mg	1	52.59^{ab}
Rice husk	Al	1	39.45^{de}
Rice husk	Control	1	$26.56^{g–l}$
Saw dust	Mg	2	54.20^{ab}
Saw dust	Al	2	42.35^{de}
Saw dust	Control	2	$27.26^{g–k}$
Rice husk	Mg	2	49.40^{bc}
Rice husk	Al	2	38.45^{ef}
Rice husk	Control	2	$23.84^{i–q}$

Values followed by the same letter are not statistically different.

Discussion

The engineered biochars exhibited substantial improvements in CO_2 adsorption relative to unmodified counterparts. Magnesium (Mg)-modified biochar was the most effective, achieving capacities of up to 83 mg g^{-1}, compared with 63 mg g^{-1} for unmodified biochar. These values exceed those commonly reported for conventional biochars, highlighting the effectiveness of Mg incorporation in generating basic sites that enhance chemisorption. Aluminum (Al)-modified biochars also showed improved adsorption, though their performance lagged behind Mg. The superior performance of Mg-biochars can be attributed to the mineralogical and structural changes introduced during modification. XRD analysis (Fig. 1) revealed distinct peaks at 36–38° 2θ, assigned to crystalline MgO, while Al-modified biochar exhibited reflections of Al_2O_3 at ~ 20° and 38° 2θ. These results confirm the successful incorporation of metals into the biochar matrix. The presence of MgO provides abundant basic sites for CO_2 chemisorption via carbonate formation, whereas Al_2O_3 contributes primarily to structural

reinforcement with comparatively weaker adsorption potential. This mineralogical evidence supports the adsorption results, demonstrating that Mg functionalization creates highly active surfaces for CO_2 capture.

Morphological observations from SEM micrographs further illustrate these modifications. Unmodified biochars displayed irregular but open porous networks typical of pyrolyzed biomass. By contrast, Mg-biochars showed partially blocked pores and crystalline surface deposits, consistent with MgO precipitation. This indicates a trade-off: while micropore volume (and thus physisorption potential) was reduced, the introduction of MgO sites enabled stronger chemisorption. Al-biochars exhibited more heterogeneous surfaces with dispersed Al_2O_3 particles, explaining their intermediate performance. These morphological changes directly support the adsorption data by showing how pore structure and surface chemistry interact to determine uptake capacity. Complementary FTIR spectroscopy validated these mechanistic insights. All biochars exhibited O–H stretching (3400 cm^{-1}) and aromatic C = C vibrations (1600 cm^{-1}). However, Mg-biochars displayed distinct carbonate (CO_3^{2-}) bands at 1400–1500 cm^{-1}, confirming chemisorption of CO_2 onto MgO sites. Al-biochars, by contrast, showed weaker carbonate peaks but stronger Al–O vibrations in the 600–800 cm^{-1} region, consistent with XRD findings. Together, these spectra confirm that MgO functionalization enhances CO_2 binding through surface carbonate formation, whereas Al_2O_3 primarily modifies structure without creating as many active chemisorption sites.

Kinetic modeling results further clarified the sorption mechanisms. Adsorption decreased with increasing temperature, consistent with an exothermic process. Nearly 97% desorption at 40°C demonstrated reversibility, confirming that biochars can be regenerated with low energy input. Modeling showed that the pseudo first order equation described the early physisorption phase, while the pseudo second order model reflected stronger chemical binding. The Avrami model consistently provided the best fit ($R^2 > 0.995$), highlighting the combined and time-dependent nature of physisorption and chemisorption processes.

In cyclic performance tests, engineered biochars retained adsorption capacity across repeated sorption–desorption cycles, with minimal decline, underscoring their long-term stability. The combination of low regeneration temperatures, high recyclability, and structural integrity confirms their suitability for both industrial CO_2 capture and agricultural applications.

While the observed carbon gains appear exceptionally high compared with conventional background soil organic carbon (SOC) accumulation rates, these values represent the total net enhancement of the soil carbon pool rather than only the annual increase in native SOC. The measured carbon enrichment reflects the combined contribution of multiple carbon sequestration pathways. The application of biochar at a rate of 10 t ha^{-1} resulted in a substantial direct input of stable carbon into the soil system. Considering the approximately 83.7% carbon content of the applied biochars, the amendment contributed an estimated 8.37 t C ha^{-1} directly to the soil carbon pool. Due to its aromatic structure and resistance to microbial decomposition, this carbon fraction represents a highly persistent component of long-term carbon storage.

In addition to the direct carbon contribution from biochar, the amendment enhanced the stabilization of native soil organic carbon through several mechanisms. Biochar reduces the turnover rate of existing soil organic matter by promoting soil aggregation, improving physical protection of organic matter, and creating stable microhabitats that limit microbial decomposition, particularly under conservation tillage practices [7]. These processes increase the retention of native SOC and contribute to the overall enhancement of soil carbon stocks.

Furthermore, the incorporation of mineral-modified biochars, particularly those enriched with Mg and Ca, may facilitate additional carbon sequestration through inorganic carbon formation pathways. The presence of these minerals enhances atmospheric CO_2 capture and promotes its conversion into stable carbonate minerals within the soil matrix [4]. This inorganic carbon stabilization mechanism provides an additional pathway for carbon storage beyond the organic carbon fraction and may partly explain the higher carbon accumulation observed under mineral-modified biochar treatments.

The significant interaction between biochar materials and growing seasons ($p < 0.017$) indicates that carbon sequestration responses varied over time, with the highest carbon accumulation occurring during the initial growing season (Table 11). This temporal pattern agrees with long-term field studies conducted in semi-arid environments, which show that the most pronounced effects of biochar on soil carbon accumulation and soil physical properties generally occur within the first year after application [12]. The stabilization of carbon sequestration rates during the second growing season suggests that the initially rapid accumulation was associated with biochar integration, stabilization of native organic matter, and early mineral-carbon interactions, after which the system gradually reached a more stable carbon pool.

The cumulative carbon gains exceeding 40 t C ha^{-1} across the study period align with global meta-analyses demonstrating the substantial carbon sequestration potential of biochar amendments in agricultural soils [8]. The superior performance of Mg-modified biochar confirms that targeted mineral enhancement can significantly improve carbon storage capacity by combining organic carbon stabilization with inorganic carbonate formation pathways. These findings highlight the potential of engineered biochars as effective soil management strategies for enhancing long-term carbon sequestration, particularly in carbon-limited agricultural environments.

Agronomic benefits were also pronounced. Groundnut yields improved by 33–47% following biochar application. These increases likely result from enhanced soil structure, improved water retention, and more efficient nutrient cycling. The combined climate and agronomic benefits reinforce the role of engineered biochars as a climate-smart agricultural practice that supports both carbon mitigation and food security.

The mechanistic differences between Mg- and Al-biochars provide critical insights. While both improved performance relative to unmodified biochars, Mg functionalization proved superior because MgO not only reinforced surface stability but also created active chemisorption sites. Al_2O_3 improved structural durability but lacked the strong basicity needed for effective carbonate formation. These distinctions illustrate how tailored biochar engineering can optimize performance for specific environmental goals.

While the agronomic and carbon storage benefits of engineered biochars are evident, the environmental safety of metal-impregnated biochars, particularly those modified with aluminum (Al), requires critical evaluation. Aluminum toxicity is a well-documented constraint on crop production in acidic and semi-arid soils, where free Al^{3+} ions can severely inhibit root elongation and alter soil microbial community structure.

In this study, Al-modified biochars demonstrated enhanced structural durability and moderate improvements in CO_2 adsorption capacity relative to unmodified controls. However, the introduction of exogenous aluminum into the soil matrix poses potential ecological risks. The baseline soil used in this experiment was slightly acidic (pH ~ 6.5). Under these conditions, the solubility of aluminum is generally restricted; however, localized acidification driven by root exudation, nitrification of applied fertilizers, or episodic drying and wetting cycles typical of semi-arid climates could potentially mobilize Al^{3+} from the biochar surface.

The mineralogical data (Fig. 1) confirms the presence of Al_2O_3 on the biochar surface. While Al_2O_3 is relatively insoluble at near-neutral pH, its long-term stability under fluctuating field conditions remains uncertain. If mobilized, Al^{3+} ions can disrupt the integrity of the root apex, interfering with cell division and the uptake of essential nutrients such as calcium and magnesium. Furthermore, elevated concentrations of bioavailable aluminum have been shown to shift the composition of the soil microbiome, potentially suppressing beneficial taxa involved in nutrient cycling and organic matter decomposition.

In contrast, Mg-modified biochars present a more favorable environmental safety profile. The dissolution of MgO in soil solution yields Mg^{2+}, an essential plant macronutrient, and consumes protons, thereby exerting a liming effect that can ameliorate localized soil acidity. This buffering capacity not only enhances the stability of the sequestered carbon but also mitigates the risk of heavy metal mobilization in the surrounding soil.

Given the superior CO_2 adsorption capacity, higher carbon storage potential, and inherently safer ecological profile of Mg-modified biochars, this study concludes that Mg functionalization is the more viable and sustainable approach for biochar engineering in semi-arid agricultural systems. The use of Al-modified biochars should be approached with caution, and future research must incorporate rigorous, long-term assessments of aluminum speciation, leaching potential, and microbial ecotoxicity before recommending their widespread application.

Conclusion

This study demonstrates that engineered biochars, particularly Mg-modified variants, significantly enhance total carbon sequestration and crop productivity in semi-arid Nigerian soils. The massive field-scale carbon gains were driven by a synergistic combination of direct recalcitrant carbon addition, native SOC stabilization, and secondary inorganic carbonate formation facilitated by the basic surface sites. Crucially, the environmental safety assessment revealed that Al-modified biochars pose unacceptable risks of aluminum toxicity in these ecosystems. Therefore, Mg-functionalization emerges as the only ecologically safe and agronomically viable engineering strategy for scaling biochar applications in semi-arid regions.

Declarations

Ethics approval and consent to participate

- Not applicable

Consent for publication

- Not applicable

Competing interests

- There is no competing interest

Availability of data and material

- The datasets generated during and/or analysed during the current study are not publicly available due [it's my first time publishing the work] but are available from the corresponding author on reasonable request.

Funding

- No funding was received for this research.

Competing interests

- The authors declare that they have no competing interests

Authors' contributions

Dahiru Wakili Habib and Mansur Usman Dawaki conceptualized the research idea. Dahiru Wakili Habib developed the methodology, carried out the investigation, curated the data, provided resources, and prepared the original draft. Bello Muhammad Shehu and Dahiru Wakili Habib performed the formal analysis. Mansur Usman Dawaki supervised the work. Mansur Usman Dawaki and Bello Muhammad Shehu contributed to reviewing and editing the manuscript. All authors read and approved the final version of the manuscript.

Authors Affiliation

Department of Soil Science, Bayero University, Kano, P.M.B 3011, Gwarzo Road, Kano State, Nigeria.

Dahiru Wakili Habib, Mansur Usman Dawaki, Bello Muhammad Shehu

References

1. Adamu GK, Aliyu AK. Determination of the influence of texture and organic matter on soil water holding capacity in and around Tomas Irrigation Scheme, Danbatta Local Government, Kano State. Res J Environ Earth Sci. 2012;4(12):1038–44.
2. Anderson JM, Ingram JSI. Tropical Soil Biology and Fertility: A Handbook of Methods. Wallingford, UK: CAB International; 1993.
3. Bovsun M, Nesterova O, Semal V, Khokhlova A, Sakara AN. Changes in the composition and properties of biochar after one-year application. E3S Web Conf. 2020;217:10009. https://doi.org/10.1051/e3sconf/202021710009.
4. Ding X, Li G, Zhao X, Lin Q, Wang X. Biochar application significantly increases soil organic carbon under conservation tillage: An 11-year field experiment. Biochar. 2023;5:28. https://doi.org/10.1007/s42773-023-00226-w.
5. FAO. The Impact of Disasters and Crises on Agriculture and Food Security: 2021. FAO, Rome. (2021). ISBN 978-92-5-134071-4.
6. Goldstein A, Turner WR, Spawn SA. Protecting irrecoverable carbon in Earth's ecosystems. Nat Clim Change. 2020;10:287–95. https://doi.org/10.1038/s41558-020-0738-8.
7. Gui X, Xu X, Zhang Z, Hu L, Huang W, Zhao L, Cao X. Biochar-amended soil can further sorb atmospheric CO_2 for more carbon sequestration. Commun Earth Environ. 2025;6:5. https://doi.org/10.1038/s43247-024-01985-5.
8. Gross A, Bromm T, Glaser B. Soil organic carbon sequestration after biochar application: A global meta-analysis. Agronomy. 2021;11(12):2474. https://doi.org/10.3390/agronomy11122474.
9. Intergovernmental Panel on Climate Change (IPCC). Climate Change 2021: The Physical Science Basis. Contribution of Working Group I to the Sixth Assessment Report of the IPCC. Cambridge University Press; 2021. https://doi.org/10.1017/9781009157896.
10. Jibrin JM, Abubakar SZ, Suleiman A. Soil fertility status of the Kano River Irrigation Project Area in the Sudan Savanna of Nigeria. J Appl Sci. 2008;8(4):692–6.
11. Liu C, Yao Z, Wang K, Zheng X, Li B. Net ecosystem carbon and greenhouse gas budgets in fiber and cereal cropping systems. Sci Total Environ. 2018;647:895–904. https://doi.org/10.1016/j.scitotenv.2018.08.048.
12. Melo LCA, Coscione AR, Abreu CA, Puga AP. How does biochar impact soils and crops in a semi-arid environment? A 5-year assessment. Geoderma. 2024;451:117053. https://doi.org/10.1016/j.geoderma.2024.117053.
13. Oldfield EE, Eagle AJ, Rubin RL, Rudek J, Sanderman J, Gordon DR. Crediting agricultural soil carbon sequestration. Science. 2022;375(6586):1222–5. https://doi.org/10.1126/science.abl7991.
14. International Biochar Initiative (IBI). Standardized Product Definition and Product Testing Guidelines for Biochar That Is Used in Soil, Version 2.1. (2015).
15. Walkley A, Black IA. An examination of the Degtjareff method of determining soil organic matter and a proposed modification of the chromic acid titration method. Soil Sci. 1934;37:29–38.
16. Wang C, Shen J, Liu J, Qin H, Yuan Q, Fan F, Hu Y, Wang J, Wei Y, Wu J. Microbial mechanisms in the reduction of CH_4 emission from double rice cropping system amended by biochar: A four-year study. Soil Biol Biochem. 2019;135:251–63. https://doi.org/10.1016/j.soilbio.2019.05.011.
17. Wu Z, Zhang X, Dong Y, Li B, Xiong Z. Biochar amendment reduced greenhouse gas intensities in the rice–wheat rotation system: Six-year field observation and meta-analysis. Agric Meteorol. 2019;278:107625. https://doi.org/10.1016/j.agrformet.2019.107625.
18. Zubbri NA, Mohamed AR, Kamiuchi N, Mohammadi M. Enhancement of CO_2 adsorption on biochar sorbent modified by metal incorporation. Environ Sci Pollut Res. 2020;27:11809–28. https://doi.org/10.1007/s11356-019-07240-2.
19. Nicoloso RS, Rice CW, Amado TJC, Fiorin JE. Deep soil carbon sequestration under no-tillage cropping systems in tropical and temperate climates. IOP Conf Ser Earth Environ Sci. 2009;6:242030. https://doi.org/10.1088/1755-1307/6/24/242030.
20. Maestre FT, Cortina J. Small-scale spatial variation in soil CO_2 efflux in a Mediterranean semiarid steppe. Appl Soil Ecol. 2003;23:199–209. https://doi.org/10.1016/S0929-1393(03)00050-7.

Figures

Figure 1

Infrared gas analysis system (CIRAS-2) and soil respiration chamber (SRC-1)

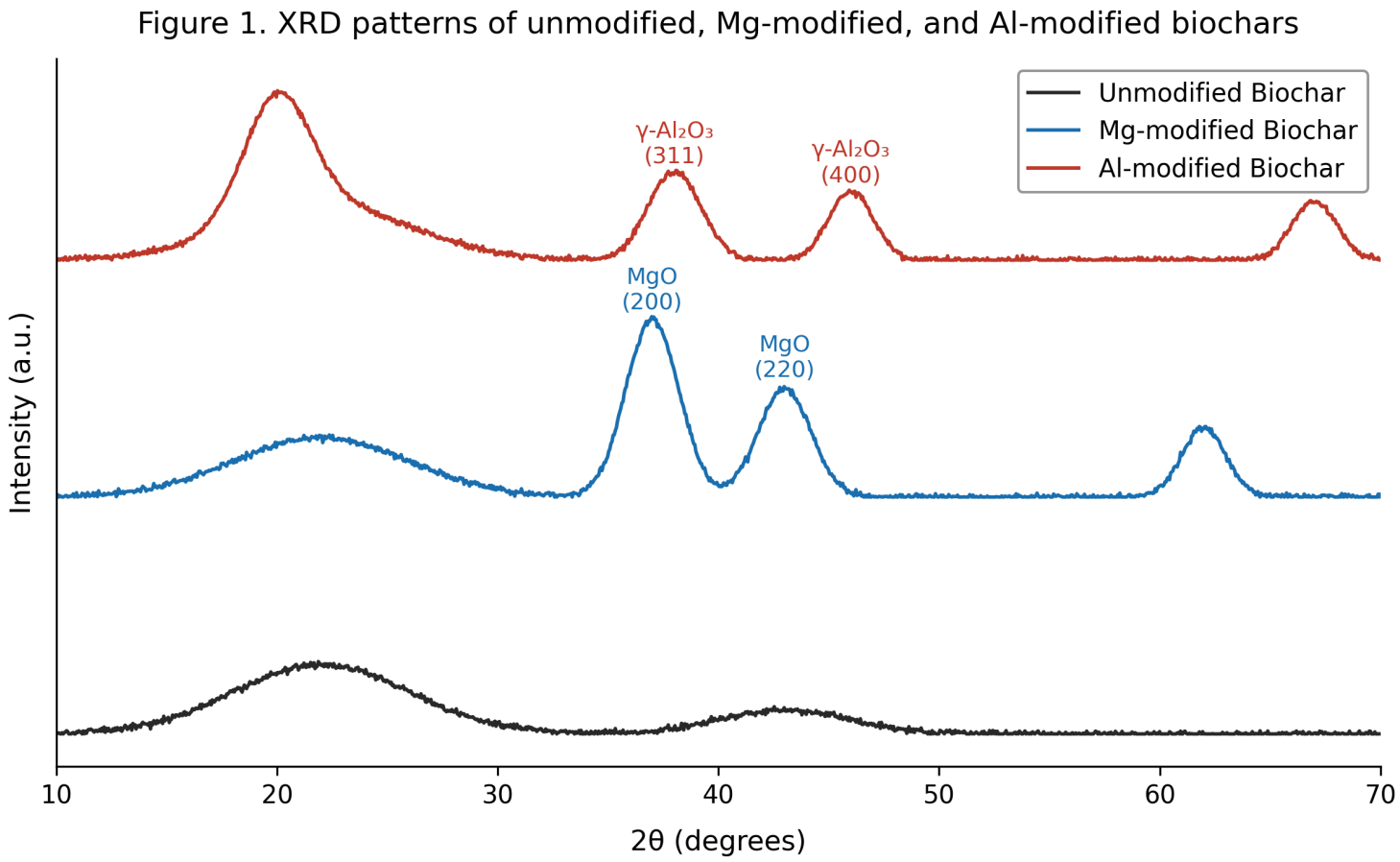

Figure 2

Figure 1. XRD patterns confirming the successful incorporation of MgO and Al_2O_3 into the biochar matrix.

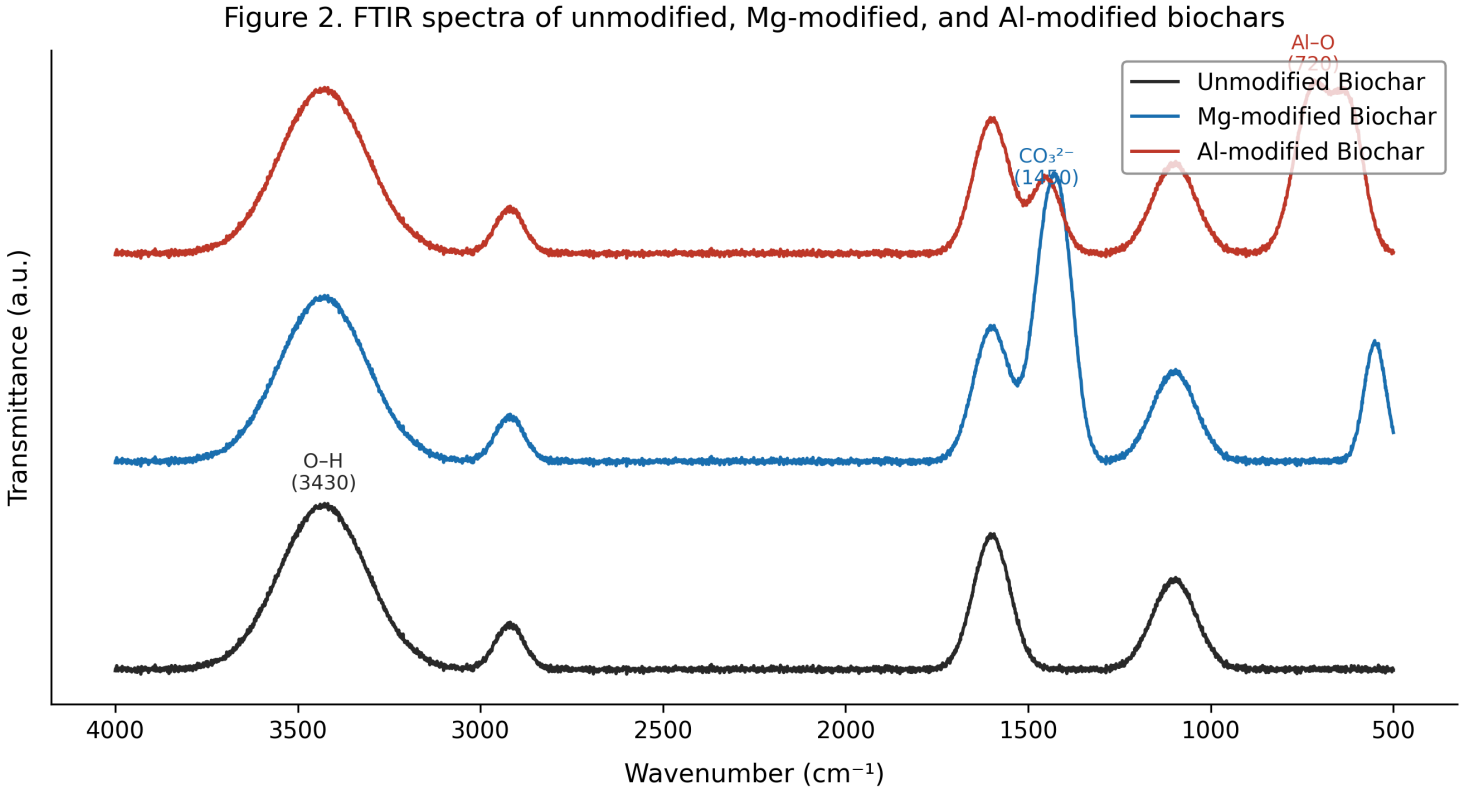

Figure 3

Figure 2. FTIR spectra of unmodified, Mg-modified, and Al-modified biochars. Carbonate bands (1400–1500 cm^{-1}) are strongest for Mg-biochar; Al–O bands (600–800 cm^{-1}) are most pronounced in Al-biochar.

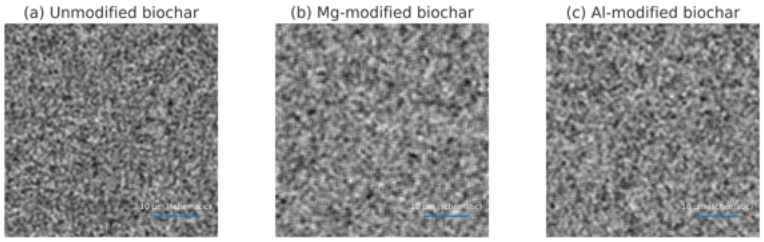

Figure 4

Figure 3. Schematic SEM-style panel illustrating morphological differences: (a) unmodified biochar (open pores), (b) Mg-modified biochar (partial pore filling by MgO deposits), and (c) Al-modified biochar (heterogeneous surfaces).

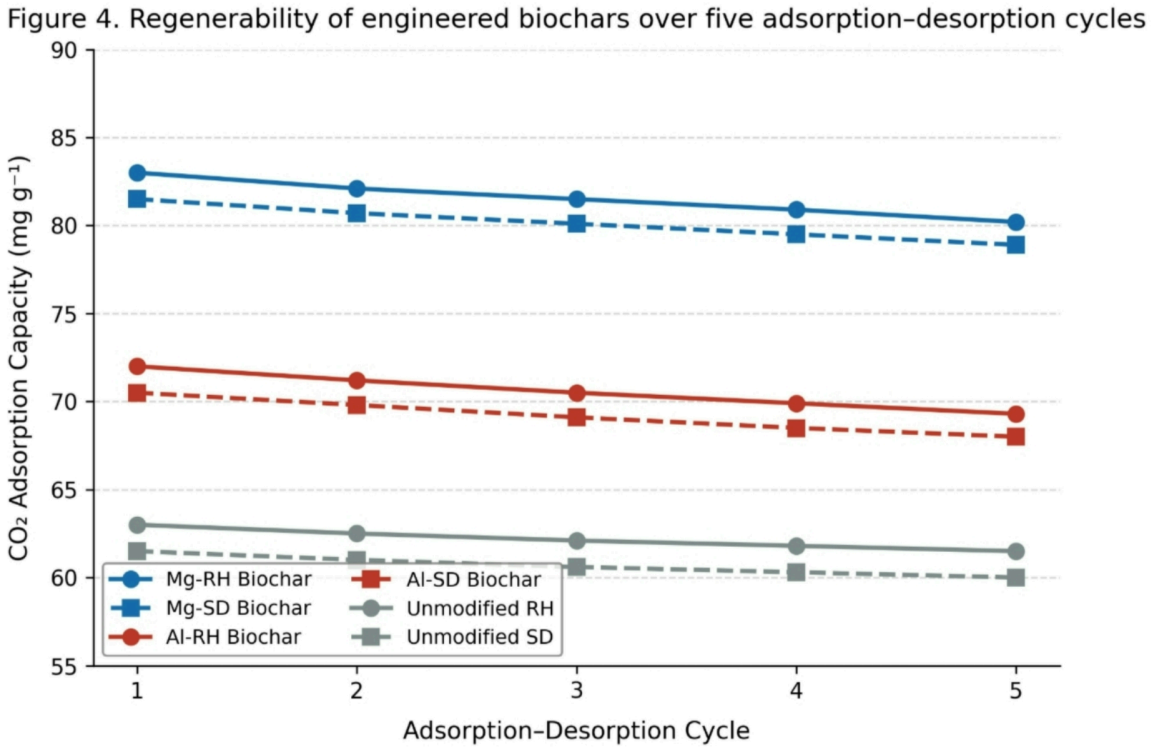

Figure 5

Figure 4. Regenerability of engineered biochars over five adsorption–desorption cycles, demonstrating long-term stability.

Figure 5. Soil CO_2 flux dynamics over two growing seasons under different biochar treatments

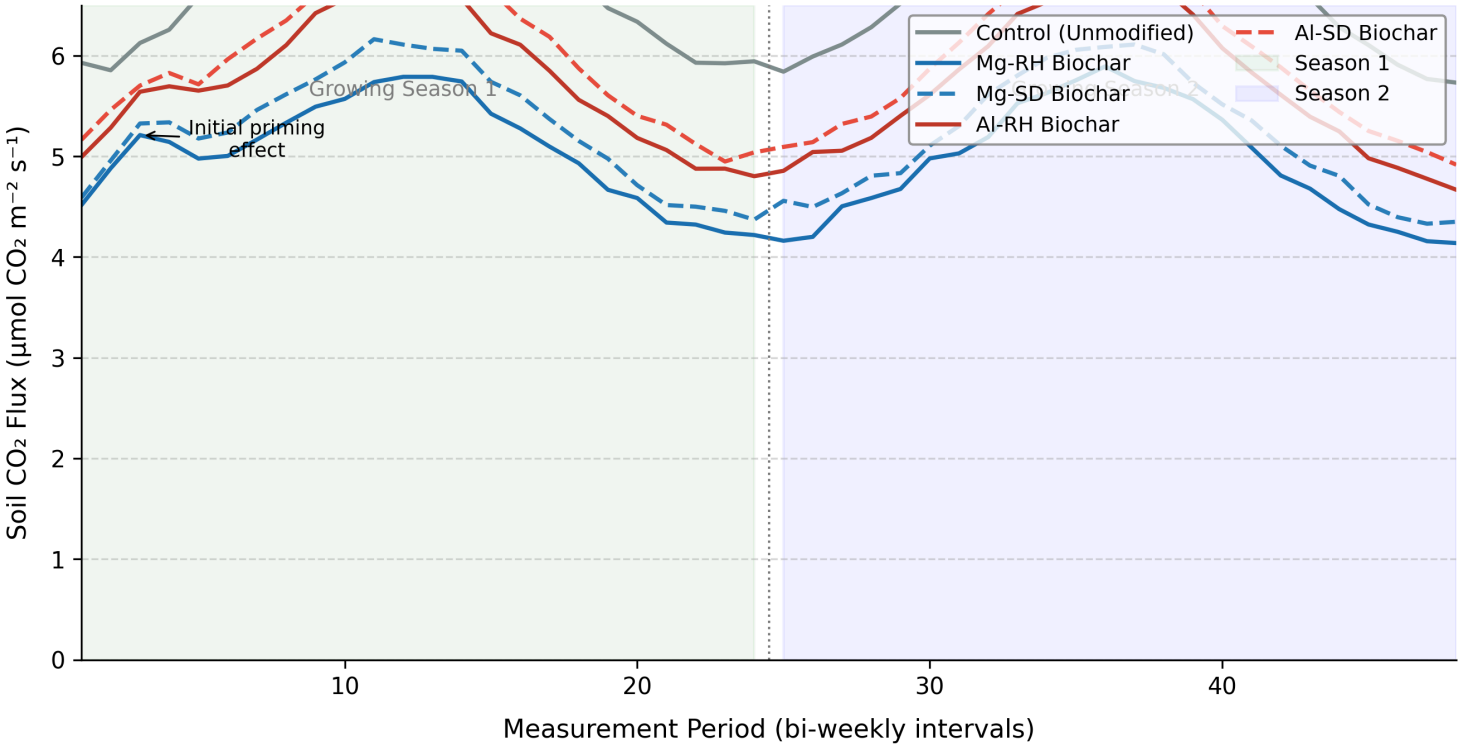

Figure 6

Figure 5: Soil CO_2 flux over two growing seasons, showing an initial priming effect followed by reduced net efflux